A reference material for establishing uncertainties in full-field displacement measurements

OPEN ACCESS
IOP Publishing
Measurement Science and Technology
Meas. Sci. Technol. **26** (2015) 075004 (13pp)
doi:10.1088/0957-0233/26/7/075004

A reference material for establishing uncertainties in full-field displacement measurements

E Hack[1], X Lin[2], E A Patterson[2] and C M Sebastian[2]

[1] Laboratory of Reliability Science and Technology, EMPA, Dübendorf, Switzerland
[2] Centre for Materials and Structures, School of Engineering, University of Liverpool, UK

E-mail: c.sebastian@liv.ac.uk

Received 28 January 2015, revised 17 April 2015
Accepted for publication 1 May 2015
Published 12 June 2015

Abstract

A simple reference material for establishing the minimum measurement uncertainty of optical systems for measuring 3D surface displacement fields in deforming objects is described and its use demonstrated by employing 3D digital image correlation as an exemplar technique. The reference material consists of a stepped bar, whose dimensions can be scaled to suit the application, and that can be clamped rigidly at its thick end to create an idealized cantilever. The cantilever was excited at resonance to generate out-of-plane displacements and, in a separate experiment, loaded statically in-plane to provide in-plane displacement fields. The displacements were measured using 3D digital image correlation and compared to the predicted displacement fields derived from tip deflections obtained using a calibrated transducer that provided traceability to the national standard for length. The minimum measurement uncertainties were evaluated by comparing the measured and predicted displacement fields, taking account of the uncertainties in the input parameters for the predictions. It was found that the minimum measurement uncertainties were less than 3% for the Cartesian components of displacement present during static in-plane bending and less than 3 μm for out-of-plane displacements during dynamic loading. It was concluded that this reference material was more straightforward to use, more versatile and yielded comparable results relative to an earlier design.

Keywords: reference material, measurement uncertainty, calibration, digital image correlation

(Some figures may appear in colour only in the online journal)

1. Introduction

Most modern engineering analysis is based on computational models, and hence establishing confidence in and credibility of these models is essential. An important step in this process is to assess the degree to which a model is an effective 'surrogate for reality' [1] and this is usually termed as validation [2]. For instance, Oberkampf and Barone [3] have provided validation metrics that are measures of agreement between computational predictions and experimental measurements, while Sebastian *et al* [4] have provided a go/no-go approach to assessing the effectiveness of computational solid mechanics models [5]. In both these approaches, the uncertainty in the experimental measurements is a key requirement for making the assessment, and Patterson *et al* [6] proposed a reference material[3] for establishing the uncertainty associated with measurements of

[3] A 'reference material' is defined as a 'material, sufficiently homogeneous and stable with reference to specified properties, which has been established to be fit for its intended use in measurement or in examination of nominal properties' from [7].

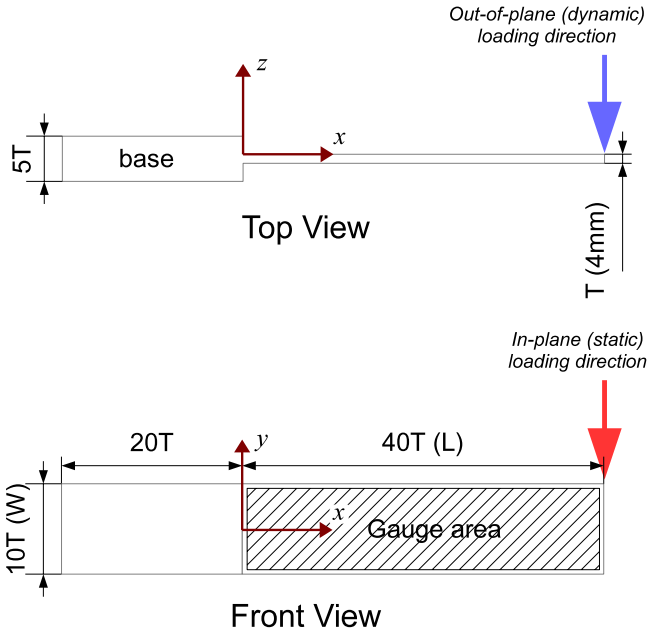

Figure 1. Geometry of the reference material with the gauge area shown shaded.

in-plane strain fields using camera-based optical instruments. The design of this reference material featured a beam subject to four-point bending within a monolithic frame, and it has been used successfully to establish measurement uncertainties for electronic speckle pattern interferometer (ESPI) [8] and digital image correlation (DIC) systems [9]. These uncertainties were found to be 34 and 18 microstrain respectively for a strain range of approximately 1000 microstrain. The geometry of the reference material used in this earlier work is complicated, which renders it difficult and expensive to manufacture and, in addition, it is unsuitable for evaluating uncertainties associated with out-of-plane or dynamic strain fields. More recently, Tan *et al* [10] and Felipe-Sesé *et al* [11] have used a cantilever beam as reference material for evaluating the uncertainties associated with the measurement of static out-of-plane displacements using a 3D DIC system and a combined fringe projection and 2D DIC system, respectively. This design of reference material, based on a cantilever, has a simple geometry, is easier to manufacture than the reference material consisting of a beam in a monolithic frame, and does not require the determination of any correction factors. In addition, the gauge area covers 66% of the overall reference material surface rather than 1% as before. Thus, this paper reports two parallel studies to evaluate the usefulness of the cantilever-design of reference material, shown in figure 1, for evaluating uncertainties associated with measurements of static in-plane displacements and dynamic out-of-plane displacements. In the former case, the cantilever-design could be considered a replacement for the design incorporating a beam in four-point bending and hence would provide a single reference material for evaluating measurement uncertainties associated with in-plane and out-of-plane displacements and strains.

The use of digital image correlation in experimental mechanics has become almost ubiquitous and so it was selected as the most relevant technique for the studies reported here. In addition to the uncertainty evaluations mentioned above there have been a number of studies of the errors associated with digital image correlation. A survey by Pan *et al* [12] discussed the basics of 2D digital image correlation including the different correlation algorithms as well as error analysis. Haddadi and Belhabib [13] divided the sources of error into two main categories: those related to experimental set-up and imaging, and those from the correlation algorithm. They attempted to quantify these sources of error by performing rigid body translations of a specimen. Various other methods have involved synthetically deforming images, either by applying a sinusoidal displacement [14, 15] or by applying the results of a finite element simulation to deform the speckle images [16–18]. Wang *et al* examined the effects of noise on 1D and 2D motion measurements [18].

There has been some analysis of uncertainty for 3D digital image correlation set-ups. Becker *et al* [19] examined the parameter calibration and resulting errors, including the lens-induced distortions resulting from short focal lengths, and the effects of camera alignment and position error have been investigated by Sutton *et al* [20] and Lava *et al* [21]. Siebert *et al* [22] compared 3D DIC to ESPI and strain gauges in a tensile test, as well as performing some limited dynamic experiments using a cantilever. Recently, Reu [23] examined the uncertainty resulting from parameter calibration by processing different subsets of a pool of several thousand images and Zappa *et al* [24] examined the effect of movement during the measurement process in high-speed digital image correlation.

The investigations highlighted above attempted to define the limits of digital image correlation when performed under laboratory conditions in a research environment but they do not provide information about the level of uncertainty in measurements obtained with a specific set-up used in a routine experiment. The provision of a reference material and associated protocol for routinely evaluating the measurement uncertainty of an optical system for measuring the full-field in-plane and out-of plane deformation of a component subject to static or dynamic loading was the objective of this study.

When digital image correlation or any other optical measurement technique, such as ESPI or shearography, is to be used in industry within a regulatory environment, e.g. the aerospace or nuclear industries, then it is usually important to perform the measurements within a standards framework in order to assist in establishing confidence in the measurements. In this context, it is relevant to consider the traceability[4] of the measurements, which is a component of a quality assurance system, and should allow an unbroken chain of comparisons or calibrations to an international reference. Previously, this unbroken chain of calibrations has been established from strain measurement to the international standard for length [6] and it is proposed to follow this precedent in this work. The need to achieve calibrations with the implication of minimizing uncertainties dictates that the strain or displacement distribution in a reference material should be relatively simple, and

[4] Traceability is defined as 'the property of a measurement result whereby the result can be related to a reference through a documented unbroken chain of calibrations, each contributing to the measurement uncertainty' [7].

the cantilever design employed here, and shown in figure 1, satisfies this requirement as has been reported previously for measurements of static out-of-plane displacements [10, 11]. The geometry of the reference material has been defined in CEN CWA 16799 [5] and was designed to be scalable, so all of the dimensions are expressed as a function of T, the cantilever thickness. The reference material has been designed with a thick base section, which is intended to be securely clamped while load or excitation is applied to the resulting cantilever. The entire face on one side of the cantilever forms the gauge area (see figure 1) on which the optical measurements are performed. The results reported here demonstrate the suitability of the reference material for evaluating uncertainties in measurements of static in-plane displacements and dynamic out-of-plane displacements.

2. Analytical descriptions

2.1. In-plane displacements

The elementary theory describing the bending of beams is based on the Euler–Bernoulli beam theory, which ignores the effect of shear deformation. The fundamental assumption of Euler–Bernoulli beam theory is plane sections that are initially perpendicular to the centroidal axis remain plane and perpendicular to the axis after deformation, which implies that the transverse shear and transverse normal effects are neglected [25]. In practice, Euler–Bernoulli beam theory is acceptable for slender beams where the effect of shear strain on the axial stress and lateral deflection is small [26]. However, when the depth of a beam is significant compared with its length, then the effect of shear deformation is not negligible and should be taken into account. In this study, the length-to-depth ratio of the cantilever in the reference material was four, which is classified as a deep beam with an appreciable effect of shear deformation. Hence, Timoshenko's beam theory, which relaxes the restrictive assumption of the Euler–Bernoulli beam theory, was used in this work and the displacements, m_x^T and m_y^T in x and y directions respectively are given by [27]

$$m_x^T = \delta_y \frac{5y(-3\nu W^2 + 2\nu y^2 + 12Lx - 3W^2 - 6x^2 + 4y^2)}{L(11\nu W^2 + 20L^2 + 12W^2)} \quad (1)$$

$$m_y^T = \delta_y \frac{(30\nu L y^2 + 11\nu W^2 x - 30\nu x y^2 + 30Lx^2 + 12W^2 x - 10x^3)}{L(11\nu W^2 + 20L^2 + 12W^2)}, \quad (2)$$

where δ_y is the tip deflection, L is the length of the cantilever, W its width and ν is Poisson's ratio and the superscript T indicates that this is a theoretical value. The coordinate system is defined in figure 1.

2.2. Out-of-plane modal displacements

For the dynamic excitation, the theoretical natural frequencies of vibration of the cantilever were found from the following [28]:

$$f_k = \frac{\lambda_k^2}{2\pi L^2}\left(\frac{EIL}{M}\right)^{\frac{1}{2}}, \quad (3)$$

where M is the mass of the cantilever. The second moment of area is defined as $I = (WT^3/12)$, which for the cantilever in the reference material where $W = 10\,\mathrm{T}$ simplified to $I = (5T^4/6)$.

The first three dimensionless natural frequency parameters, λ_k are: $\lambda_1 = 1.875$, $\lambda_2 = 4.694$ and $\lambda_3 = 7.855$. For $k > 3$ they are given by the following relation:

$$\lambda_k = (2k-1)\frac{\pi}{2}. \quad (4)$$

The modal shape of the cantilever in bending mode, k, is given by [28]:

$$(m_z^T(\xi))_k = \frac{\delta_z}{2}[\cosh\lambda_k(1-\xi) + \cos\lambda_k(1-\xi) - \phi_k(\sinh\lambda_k(1-\xi) + \sin\lambda_k(1-\xi))], \quad (5)$$

where m_z^T is the out-of-plane displacement of the cantilever in the z-direction and is a function of $\xi = x/L$. The modal shape is proportional to the measured tip amplitude δ_z, and ϕ_k is given by

$$\phi_k = \frac{\sinh\lambda_k - \sin\lambda_k}{\cosh\lambda_k + \cos\lambda_k} \quad (6)$$

the first three values of which are $\phi_1 = 0.7340$, $\phi_2 = 1.0185$ and $\phi_3 = 0.9992$.

3. Experimental procedures

Two reference materials were manufactured using a computer-controlled milling machine from a single piece of 2024 Aluminium using tolerances of 0.05 mm. The manufacture of the reference materials was relatively straightforward; however, care was taken to ensure that the surfaces were parallel and that the cantilevers were straight. It was found that this was most easily achieved by machining them with the x–y plane vertical in the milling machine and removing small amounts of material alternately from each face in increments of 0.5 mm. The geometry of the reference material was assessed by (a) measuring its dimensions using a calibrated micrometer with an uncertainty of 1.0 μm and (b) evaluating the flatness of the cantilever by using a calibrated dial gauge indicator with an expanded uncertainty of 0.89 μm to measure the height of the upper surface of the cantilever when the reference material was placed face down on a measuring table. The thickness was machined to give a variation of less than 3 μm based on the standard deviation of nine measurements across the face of the cantilever. These series of independent observations were used to establish the uncertainty in the geometric parameters of the reference material [29]. The mean value and the standard deviation were then calculated based on these measurements and the uncertainty, $u(\psi)$ of the measurand, ψ was obtained using

$$u(\psi) = \frac{s}{\sqrt{n}}, \quad (7)$$

Table 1. Dimensions and corresponding uncertainties for reference materials (RM) used for dynamic out-of-plane and in-plane measurements.

			In-plane RM		Out-of-plane RM	
Parameter	Units	Nominal value	Mean value	Uncertainty	Mean	Uncertainty
T	mm	4	4.009	0.0023	3.98	0.008
L	mm	160	160.02	0.0023	160.01	0.012
W	mm	40	40.01	0.0023	40.00	0.014
Mass	g		—	—	251.6	0.01

where s is the standard deviation of the n measurements and n (=6) is the number of measurements for the reference materials used for the in-plane and out-of-plane measurements. The results for dimensions of the two reference materials are given in table 1. The internal corners between the two sections of the reference material were cut with a new face-milling tool and had negligible radii.

Two commercial 3D digital image correlation systems (Q-400 for the in-plane, Q-450 for the out-of-plane, Dantec Dynamics, Ulm, Germany) were used for the measurements. For both DIC set-ups, the manufacturer's recommended calibration procedure [19] was followed using a supplied target which consisted of a nine by nine checkerboard-like pattern of black and white squares. At least 12 images were captured by the cameras at different orientations of the target and the software supplied with the DIC systems (Istra 4D, Dantec Dynamics) calculated a parameter uncertainty for each measurement point which was of the order of 1.0 μm for both set-ups.

3.1. In-plane measurements

For the reference material used for in-plane measurements, a thin coat of quick-drying white paint (Matt Super White 1107, Plasti-kote, UK) was sprayed onto its surface using an aerosol can, on top of which speckles were sprayed using black paint (Matt Super Black 1102, Plasti-kote, UK). The thick section of the reference material was securely clamped to an optical table such that the cantilever was horizontal with the x–y plane vertical, as shown in figure 2, which made most efficient use of the rectangular sensors in the cameras. In order to avoid errors caused by relative movements, the DIC system was also clamped to the table. A deadweight load of 51.25 kg was applied to the tip of the cantilever using a steel ring and a weight hanger such that the cantilever was subject to a bending moment in the x–y plane. The displacements of the tip and clamped end of the cantilever were measured using two calibrated dial indicators (Mitutoyo 543-392, Kawasaki-shi, Japan). The calibration certificate of the dial indicators provided the link to the continuous chain of calibrations to the international standard for length, i.e. the traceability of the measurements.

A pair of FireWire cameras (Type 1/3 sensor, 1624 × 1234 pixels) fitted with a matched pair of 12 mm fixed focal length lenses were used. The cameras were arranged such that the whole of the gauge area (figure 1) was within the field of view, resulting in a spatial resolution of 7.1 pixels mm^{-1}. A green LED light source supplied with the DIC system (Q-400) was used to illuminate the speckle pattern.

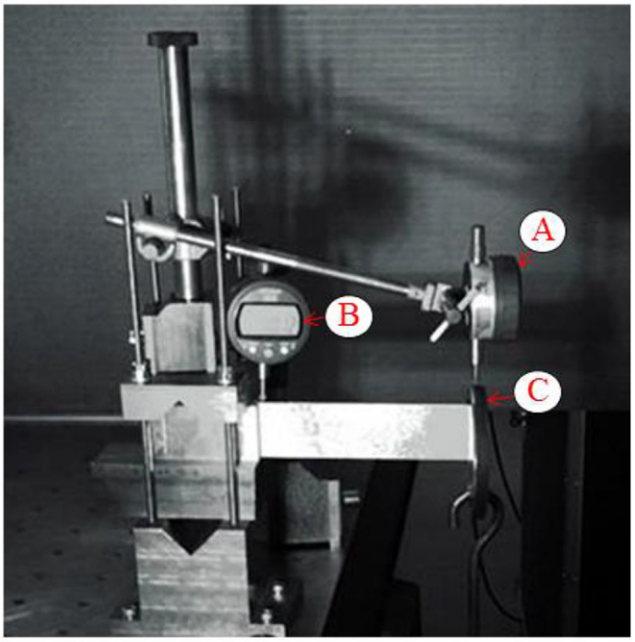

Figure 2. Experimental set-up used for in-plane loading arrangement with a dial indicator for measuring the displacement at the tip (A), a second dial indicator for controlling the displacement at the root (B) and a steel ring plus weight-hanger and weights (out of view in the photograph) used for applying dead weight (C).

3.2. Out-of-plane measurements

For the reference material used for dynamic out-of-plane measurements, a synthetic, random speckle pattern was created using a MATLAB script, with 0.5 mm diameter speckles, and printed on paper. The paper was attached to the x–y face of the cantilever using a spray adhesive. This method of generating the speckle was more reproducible than spraying paint and allowed the guidelines for speckle size given by Sutton *et al* [30] to be followed more precisely. This reference material was also clamped to the optical table in the same orientation as for static loading and the DIC system was fixed to the table, as shown in figure 3. However, in this case load was applied without physical contact using acoustic excitation in order to eliminate any rigid body motion. The excitation was provided by a subwoofer (Eurolive B1220DSP, Behringer GmbH, Kirchardt, Germany) placed behind the reference material to allow the cameras an unobstructed view. The subwoofer was driven using a sine wave output from a function generator (GW Instek GFG-8216A). The acoustic energy from the speaker caused the cantilever to vibrate at

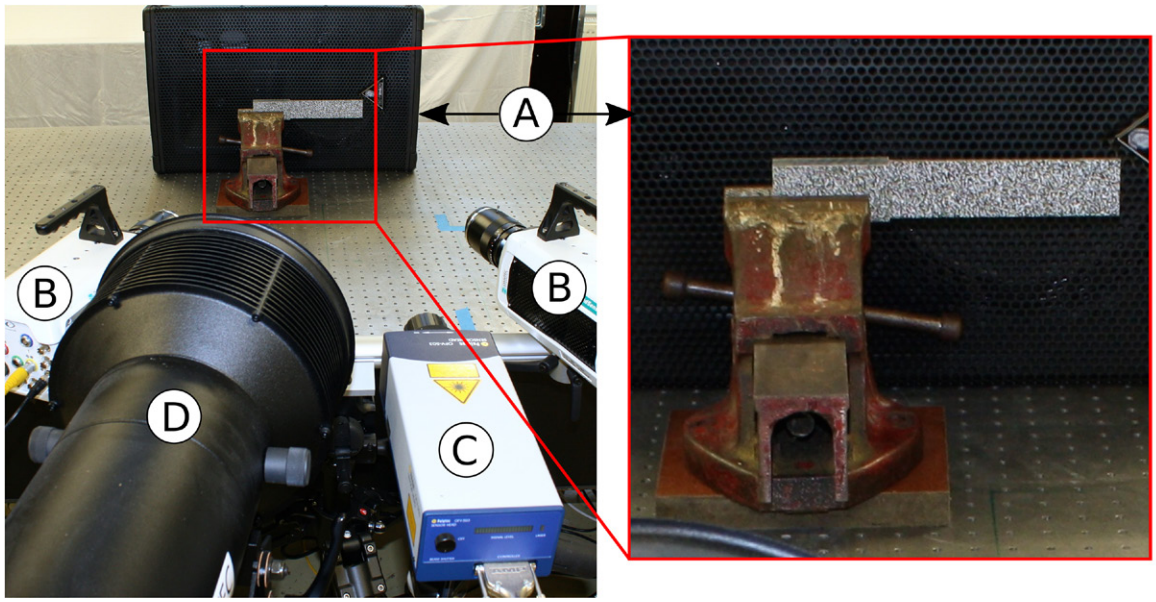

Figure 3. Experimental set-up used for dynamic out-of-plane measurements with a loudspeaker (A) used to provide the excitation, with high-speed cameras (B), a laser vibrometer (C) to measure tip deflections and provide traceability, and a white light source (D).

resonance. The amplitude of vibration could be adjusted by changing the amplitude of the signal from the function generator. A laser Doppler vibrometer (OFV-2500 controller and OFV-503 head, Polytec GmbH, Waldbronn, Germany) was used to measure the displacement of the tip of the cantilever at each of the first two natural frequencies. The vibrometer was supplied with a calibration certificate which provided the link to the chain of calibrations to the international standard for length, i.e. the traceability of the measurements.

A pair of high-speed cameras (Phantom v711, Vision Research) were used with a matched pair of 100 mm focal length lenses (Makro Planar 2/100 ZF-1, Zeiss) at a distance of 780 mm from the reference material. A white light source supplied with the DIC system (Q-450) was used to illuminate the speckle pattern. The cameras were used at an aperture stop of $f11.0$ with an exposure time of 40 μs and a capture rate of up to 12 500 frames per second. At this frame rate the resolution of the cameras was reduced from the maximum of 1200 × 800 to 1200 × 500 pixels, and approximately 90% of the horizontal detector area was used to image the length of the cantilever giving a spatial resolution of 7.1 pixels mm^{-1}.

The complexity of the dynamic measurements required attention to some additional experimental details. A small area of the speckle pattern was removed at the tip of the cantilever, revealing the reflective metal surface to enable a more reliable measurement of the tip deflection with the laser vibrometer. A caliper was used to lightly score the surface of the cantilever along the centreline at a point 3 mm from the tip, to provide a target for the vibrometer and to permit the location of the measurement to be related to the tip of the reference material during post-processing of the measurement data.

A similar procedure was used to provide an origin for the local coordinate system of the DIC data. A faint mark was made on the surface of the speckle pattern with a pencil along the centreline and at a 20 mm offset from the root of the cantilever. The reason the root of the cantilever was not used as the origin in the DIC is because the processed data did not contain information at the root due to the obstruction caused by the thick section, so a point within the available data had to be used.

Finally, the natural frequencies of the reference material were found by striking it while measuring the tip response with the laser vibrometer. The response was converted to the frequency domain by performing a fast Fourier transform (FFT), and the resulting spikes used to determine the frequencies. The frequencies were found to be 126 Hz for the first mode and 796 Hz for the second. Subsequently, while excited at each natural frequency, one hundred pairs of images were captured. A rate of 2000 frames per second was used at the first mode and 12 500 frames per second at the second mode, which resulted in approximately 15 images per cycle. The 40 μs exposure time that was used was sufficiently short to prevent any motion blur from occurring. Images of the maximum and minimum deflection were obtained by plotting the signal from the laser vibrometer and selecting images that corresponded to the peak displacements.

4. Results

Images of the gauge area of the reference materials were captured before applying load and then in the loaded or excited condition. The images were processed using the proprietary software (Istra-4D, Dantec Dynamics) provided with the DIC systems. For correlation purposes the images were subdivided into square facets with side lengths of 31 pixels for both the in-plane and out-of-plane data with an overlap of 26 and 15 pixels, respectively, which provided displacement vectors with a pitch of 5 and 14 pixels, respectively. These facet size and displacement vector pitch parameters were selected based on advice provided by Sutton *et al* [30] and prior experience in the authors' laboratory [31]. The pitch was larger

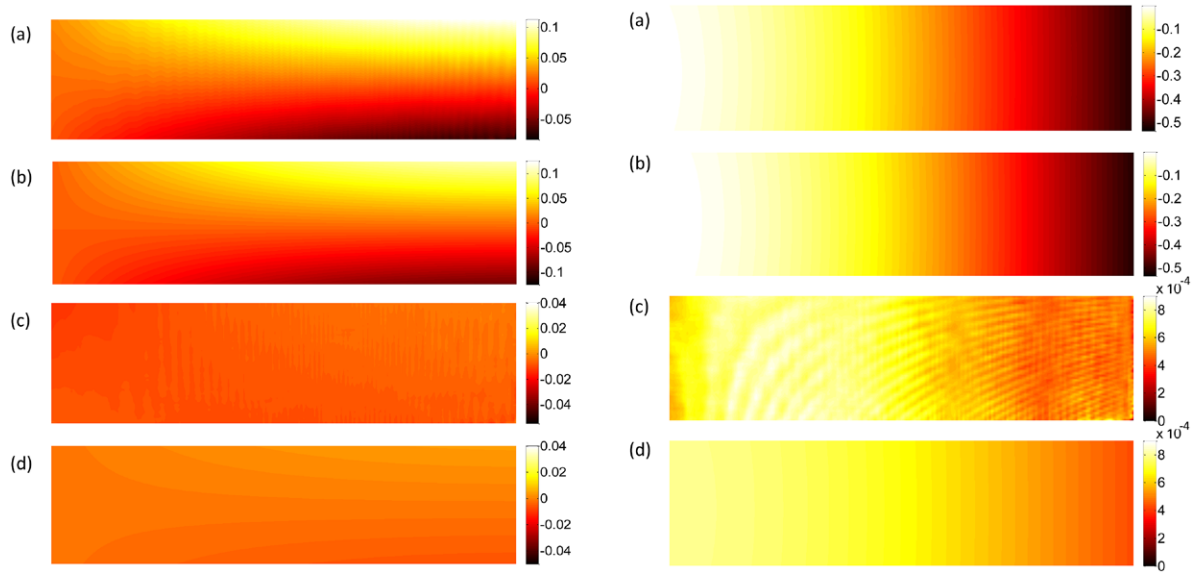

Figure 4. x (left) and y (right) displacements for the reference material subject to in-plane bending loads of 51.25 kg; the data maps are (a) measured, (b) predicted, (c) field of deviations and (d) the fitted surface based on equation (9).

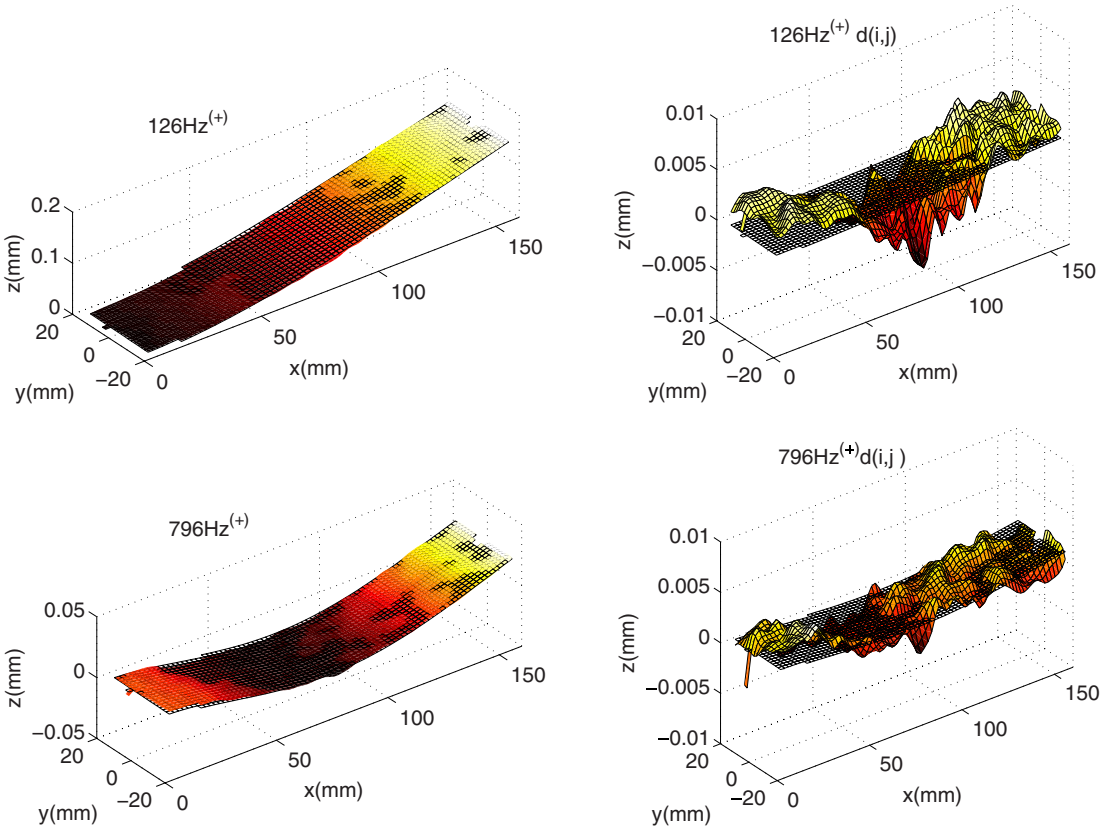

Figure 5. Predicted (mesh) and measured (solid surface) out-of-plane displacements (left column) and the corresponding field of deviations (solid surface) and the fitted surface (mesh) defined by $\alpha + \beta m^T$ (right column) for the first two natural frequencies at 126 (top) and 796 (bottom) Hz.

for the dynamic work in order to reduce the computational resource required to process the data throughout the cyclic vibration. Displacement results were imported into MATLAB using the hdf5 format and for visualization purposes, plots were produced to compare the predicted and measured displacements, which are shown in figures 4 and 5. It should be noted that for the dynamic excitation the reference material exhibited both positive (+ve) and negative (−ve) displacements about the initial undeformed shape, but only results for the positive tip displacements are shown in figure 5. It is important that the reference material should exhibit a linear relationship between the magnitudes of the applied load and

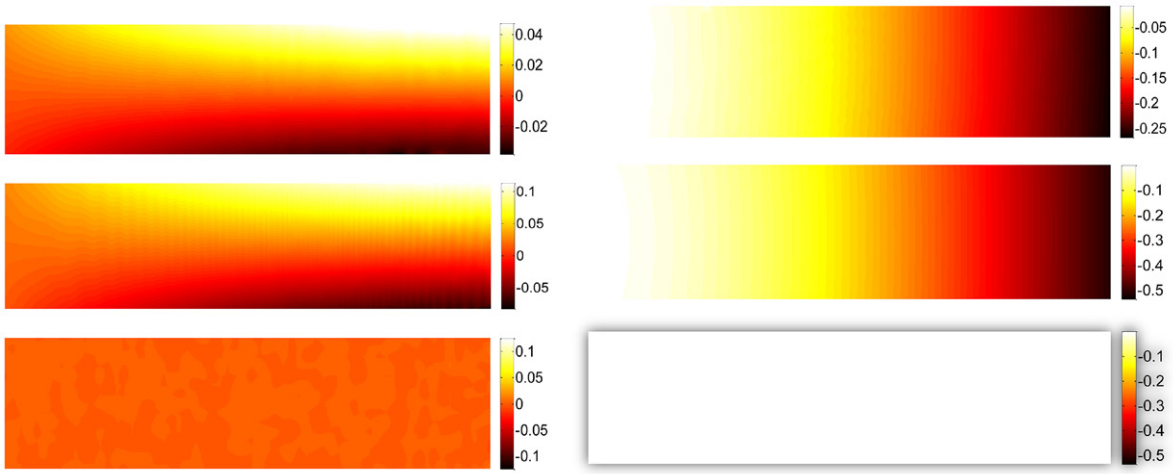

Figure 6. Measured x (left) and y (right) displacements for the reference material subject to in-plane bending at loads of 26.25 kg (top), 51.25 kg (middle) and unloading (bottom).

the displacement without any hysteresis or permanent deformation. These properties of the measurements made during dynamic loading were confirmed by comparing the displacements in the positive and negative directions and at different excitation levels for the first mode. For the in-plane static load case, displacement fields were captured at half the maximum load and immediately upon unloading as shown in figure 6 and confirmed the absence of non-linearity or hysteresis.

The field of deviations, $d(i, j)$ was also calculated following the procedure used by Patterson *et al* [6] to compare the measured values of displacement from the experiment, m^E to the predicted displacements from theory, m^T such that

$$d(i,\ j) = m^T(x_i, y_j) - m^E(x_i, y_j). \tag{8}$$

A linear least-squares fit was applied to the field of deviations to obtain two fit parameters, α and β, by minimizing the following residual [6, 32]

$$u^2(d) = \frac{1}{N-2} \sum_{i,j} \left[d(i,j) - \alpha - \beta m^T(x_i, y_j)\right]^2. \tag{9}$$

The parameters α and β can be interpreted as the systematic offset and slope error found in the regression, and are given by

$$\alpha = \frac{\sum_{i,j}(m^T)^2(x_i, y_j) \sum_{i,j} d(i,j) - \sum_{i,j} m^T(x_i, y_j) \sum_{i,j} m^T(x_i, y_j) d(i,j)}{N \sum_{i,j} (m^T)^2(x_i, y_j) - \left(\sum_{i,j} m^T(x_i, y_j)\right)^2} \tag{10}$$

and

$$\beta = \frac{N \sum_{i,j} m^T(x_i, y_j) d(i,j) - \sum_{i,j} m^T(x_i, y_j) \sum_{i,j} d(i,j)}{N \sum_{i,j} (m^T)^2(x_i, y_j) - \left(\sum_{i,j} m^T(x_i, y_j)\right)^2}. \tag{11}$$

The residual in equation (9) describes the random component of the deviations. $u(d)$ is the residual standard deviation of the regression. The predicted values, m^T were either the in-plane m_x^T and m_y^T displacements in the x and y-directions predicted from equations (1) and (2) respectively, or the out-of-plane displacements, $(m_z^T)_k$ at resonant frequency k, predicted from equation (5). The field of deviations and the corresponding surfaces described by $\alpha + \beta m^T$ are also plotted in figures 4 and 5 for all of the load cases considered.

The mean square residual deviation, $u^2(d)$, was found from

$$u^2(d) = \frac{1}{N-2} \sum_{i,j} \left[d(i,j)\right]^2 - \alpha^2 - 2\alpha\beta \frac{1}{N} \sum_{i,j} m^T(x,y) - \beta^2 \frac{1}{N} \sum_{i,j} (m^T)^2(x,y) \tag{12}$$

and used to calculate the uncertainties of the fit parameters, $u(\alpha)$ and $u(\beta)$

$$u(\alpha) = u(d) \sqrt{\frac{\sum_{i,j}(m^T)^2(x_i, y_j)}{N \sum_{i,j} (m^T)^2(x_i, y_j) - \left(\sum_{i,j} m^T(x_i, y_j)\right)^2}} \tag{13}$$

$$u(\beta) = u(d) \sqrt{\frac{1}{N \sum_{i,j} (m^T)^2(x_i, y_j) - \left(\sum_{i,j} m^T(x_i, y_j)\right)^2}}. \tag{14}$$

The values of α and β along with their associated uncertainty are shown in table 2.

Patterson *et al* [6] refer to the total uncertainty found from measurements of the deformation of the reference material, as the calibration uncertainty, u_{cal}. This *calibration*[5] is not connected to the parameter calibration routinely performed

[5] In the context of this paper, calibration is defined as an 'operation that, under specific conditions, in a first step, establishes a relation between the quantity values with measurement uncertainties provided by measurement standards and corresponding indications with associated measurements uncertainties and, in a second step, uses this information to establish a relation for obtaining a measurement result from an indication' from [7].

Table 2. Fit parameters α and β together with the associated uncertainties for each load condition considered. The abbreviation +ve and –ve in the measurand column differentiates between displacement measurements made in the positive and negative z-directions.

		Measurand	α (μm)	$u(\alpha)$ (μm)	β	$u(\beta)$
In-plane loading (51.25 kg)		m_x	−1.58	0.03	0.0512	6.91e − 6
		m_y	0.798	0.001	0.0007	3.583e − 8
Out-of-plane	1st mode 126 Hz 90 μm max. disp.	+ve m_z	0.5	0.09	−0.0066	3.06e − 5
		−ve m_z	−0.5	0.08	−0.0092	2.77e − 5
	1st mode 126 Hz 290 μm max. disp.	+ve m_z	0.4	0.07	0.0033	7.66e − 5
		−ve m_z	0.4	0.04	−0.0099	4.22e − 5
	2nd mode 796 Hz 42 μm max. disp.	+ve m_z	−0.3	0.03	−0.048	7.11e − 5
		−ve m_z	0.2	0.05	0.077	1.20e − 4

in DIC to establish the system parameters. The calibration uncertainty can be considered to be the minimum measurement uncertainty that the measurement system can achieve and in subsequent measurements on more complex components the measurement uncertainty would usually be larger than this minimum value. Since no independent values for the measurement uncertainty of DIC are available—in fact it is the purpose of this work to obtain these—the calibration uncertainty for a measurand, m^E is the combination of its residual standard deviation from the comparison to the reference material, $u(d)$ from equation (12) and the corresponding uncertainty in the predicted displacements, $u(m^T)$, which previously has been referred to as the uncertainty in the reference material, u_{RM} [5, 6, 8, 9], such that

$$u_{\mathrm{meas}}(m) = \sqrt{u^2(d) + u^2(m^T)}. \tag{15}$$

There are several sources of uncertainty that contribute to the uncertainty in the predicted deformed shape, $u(m^T)$, and these are different for the in-plane bending case, i.e. $u(m_x^T)$ and $u(m_y^T)$, and for the modal shapes, $u(m_z^T)$. In the in-plane, static case they are a combination of (a) the uncertainty in the measurement performed with the calibrated dial indicator (0.61 μm), $u(\delta)$, which in turn was a combination of the calibration uncertainty from the calibration certificate and the reading uncertainty; (b) the uncertainty in mapping the measured points to the theoretical positions in the x–y plane, or the relative positioning uncertainty, $u(\xi)$ for which a reasonable estimate was taken as one pixel on the sensor, or $u(\xi) = L/K$, where K is the number of pixels that image the length of the cantilever, and gave an uncertainty of approximately 1 μm; (c) the uncertainties in the dimensions of the reference material (see table 1); as well as (d) the Poisson's ratio which was assumed to be 10% based on the value used in Ma *et al*'s study [33]. The law of propagation of uncertainties based on the *Guide to the Expression of Uncertainty in Measurement* [32] was used to combine these uncertainties to yield the following expressions for the in-plane bending case, based on equations (1) and (2):

$$u^2(m_x^T) = \left(\frac{\partial_y m_x}{\partial\delta}\right)^2 u^2(\delta_y) + \left(\frac{\partial m_x}{\partial L}\right)^2 u^2(L) + \left(\frac{\partial m_x}{\partial W}\right)^2 u^2(W) + \left(\frac{\partial m_x}{\partial \nu}\right)^2 u^2(\nu) + \left(\frac{\partial m_x}{\partial x}\right)^2 u^2(\xi_x) + \left(\frac{\partial m_x}{\partial y}\right)^2 u^2(\xi_y) \tag{16}$$

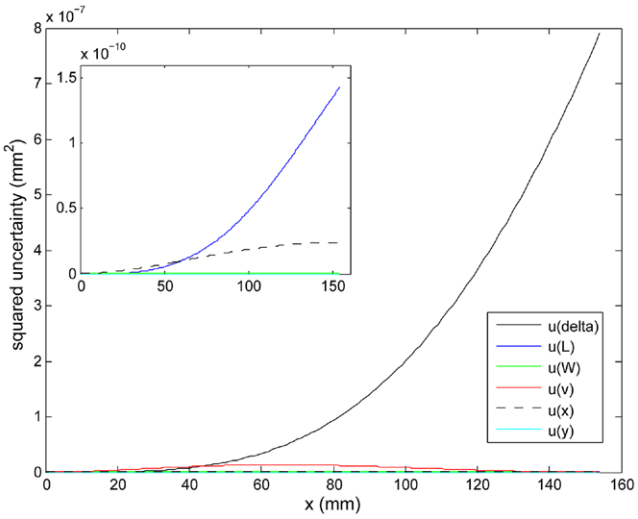

Figure 7. Plot of the contributions to the uncertainty in the theoretical prediction of the displacement, m_y^T induced by in-plane bending as a function of distance along the cantilever based on the functions provided in the appendix.

$$u^2(m_y^T) = \left(\frac{\partial_y m_y}{\partial\delta}\right)^2 u^2(\delta_y) + \left(\frac{\partial m_y}{\partial L}\right)^2 u^2(L) + \left(\frac{\partial m_y}{\partial W}\right)^2 u^2(W) + \left(\frac{\partial m_y}{\partial \nu}\right)^2 u^2(\nu) + \left(\frac{\partial m_y}{\partial x}\right)^2 u^2(\xi_x) + \left(\frac{\partial m_y}{\partial y}\right)^2 u^2(\xi_y), \tag{17}$$

where the expressions for the partial derivatives (weight factors) are listed in the appendix and their contribution to the combined uncertainty is shown in figure 7. Note that the partial derivatives are all functions of m^T, which prevents a simple tabular compilation highlighting the relative contributions.

In the out-of-plane case, the geometry and material of the reference material has no influence and hence, based on equation (5), the combined uncertainty is given by:

$$u^2((m_z^T)_k) = \left[\frac{u^2(\delta_z)}{{\delta_z}^2} + (\lambda_k\phi_k)^2 u^2(\xi)\right](m_z^T)_k^2 + u^2(\xi)\left(\frac{\delta_z}{2}\lambda_k\right)^2 \times [\sinh\lambda_k(1-\xi) - \sin\lambda_k(1-\xi) - \phi_k(\cosh\lambda_k(1-\xi) + \cos\lambda_k(1-\xi))]^2. \tag{18}$$

The uncertainties arising from the measurement made with the vibrometer and the relative positioning error were found to be both 1 μm using the same approach as for the in-plane case.

Table 3. Summary of uncertainty results for each of the measurands considered, where $u(d)$ is mean residual uncertainty from the measurements, $u(m^T)$ is the uncertainty in the theoretical values and $u_{cal}(m)$ is the combined uncertainty.

			Measurand	$u(d)$ (μm)	$u(m^T)$ (μm)	$u_{cal}(m)$ (μm)	$\hat{m}$ (μm)	Relative uncertainty (%)
Reference material shown in figure 1	In-plane loading (51.25 kg)		m_x	3.20	0.12	3.20	239	1.3
			m_y	0.064	0.469	0.474	516	0.1
	Out-of-plane	1st mode 126 Hz 290 μm max. displ.	+ ve m_z	2.1	2.0	2.9	290	1.0
			− ve m_z	1.9	2.0	2.8	290	1.0
		1st mode 126 Hz 90 μm max. displ.	+ ve m_z	1.6	2.0	2.5	90	2.8
			− ve m_z	0.9	2.0	2.2	90	2.4
		2nd mode 796 Hz 42 μm max. displ.	+ ve m_z	1.1	1.9	2.2	42	5.2
			− ve m_z	1.6	1.9	2.5	42	6.0
Cantilever RM [11]	Static in-plane		m_x	—	—	8.3	50	16
	Static out-of-plane		m_z	—	—	23.8	1000	2.4
SPOTS RM [9] In-plane			strain	—	—	—	—	1.4–4.8
SPOTS RM [8] In-plane			strain	—	—	—	—	2.2–6.2

The values found using equations (12) and (15)–(18) are given in table 3 for the largest deformation values, $\hat{m}$. It is difficult to draw any conclusions about the quality of these data from their values alone, and so following previous investigators [6, 8, 9] the results are shown graphically in figures 8 and 9 as functions of the measurand, i.e. the expanded uncertainty in the theoretical displacements, $\pm 2u(m^T)$ is plotted as a function of m^T (solid lines) together with the field of deviations, represented by $\alpha + \beta m^T \pm 2u(d)$ (dashed lines). When the area bounded by the latter is separated from the area bounded by the former, i.e. there is no overlap for all values of m^T, then the measurement system is not set-up satisfactorily and requires some adjustment or tuning. All of the plots in figures 8 and 9 show an overlap of these two areas, so it can be assumed that the measured data contained no systematic deviation but only random errors or noise.

5. Discussion

The focus of this study is to assess the utility of a proposed design of reference material for establishing the measurement uncertainty of optical systems capable of measuring in-plane and out-of-plane deformations of components subject to static and dynamic loading. In metrology, this process is known as calibration (see footnote 5) [7]. In this study, two systems based on 3D digital image correlation have been employed to demonstrate this utility and it is important to distinguish between the parameter calibration routinely performed as part of a DIC measurement and the measurement uncertainty calibration that is the subject of this study. 3D digital image correlation was selected in this study because it is widely used today; however, the reference material and procedure described can be employed with any technique for measuring full-field deformations, including for instance reflection photoelasticity or ESPI [8]. Many researchers have considered the errors inherent in digital image correlation [12–18] but that is not the purpose of this investigation. Instead, the objective was to investigate a generic approach to establishing the level of uncertainty associated with a particular measurement set-up. The Standardization Project for Optical Techniques of Strain measurement (SPOTS) sought to address this issue and developed procedures for the calibration and evaluation of optical systems capable of measuring static in-plane strain fields [6] and followed the ISO/IEC Guide to the expression of uncertainty in measurements (GUM) [32]. The reference material designed in SPOTS has one major advantage, which is the reproducibility of the results; however, it has a number of significant drawbacks that include: limitation to in-plane and static strain fields, difficulty of manufacture due to its complex shape, unfavourable ratio of gauge area to overall size, and the need to determine correction factors. Hence, this study has considered an alternative design which resolves all of these issues by being easier to manufacture as a consequence of its simpler shape (figure 1), having analytical descriptions of its deformation that do not require correction or adjustment to account for the loading or boundary conditions, and permitting static loading in-plane or out-of-plane as well as dynamic loading. In both this and the SPOTS reference material traceability to the international standard for length is achieved using a calibrated displacement transducer to make a point measurement of a relative displacement, that is, between the two halves of the monolithic specimen in the SPOTS reference material, between the stationary, rigid optical table in the current study for the in-plane case and between the stationary and displaced position in the dynamic case. A calibrated dial gauge was used in the former two cases and a calibrated vibrometer in the latter case.

Since the reference material employed in this study is proposed as an alternative to the SPOTS reference material [6], it is appropriate to compare the level of uncertainty obtained when using both reference materials. The cantilever reference material has been used previously by Tan *et al* [10], who do not provide sufficient displacement data for a detailed comparison because they calibrated for strain, and by Felipe-Sesé *et al* [11] whose data is included in table 3. Felipe-Sesé *et al* subjected the cantilever reference material to a static out-of-plane load and assessed the measurement uncertainty for both in-plane and out-of-plane displacements of their integrated

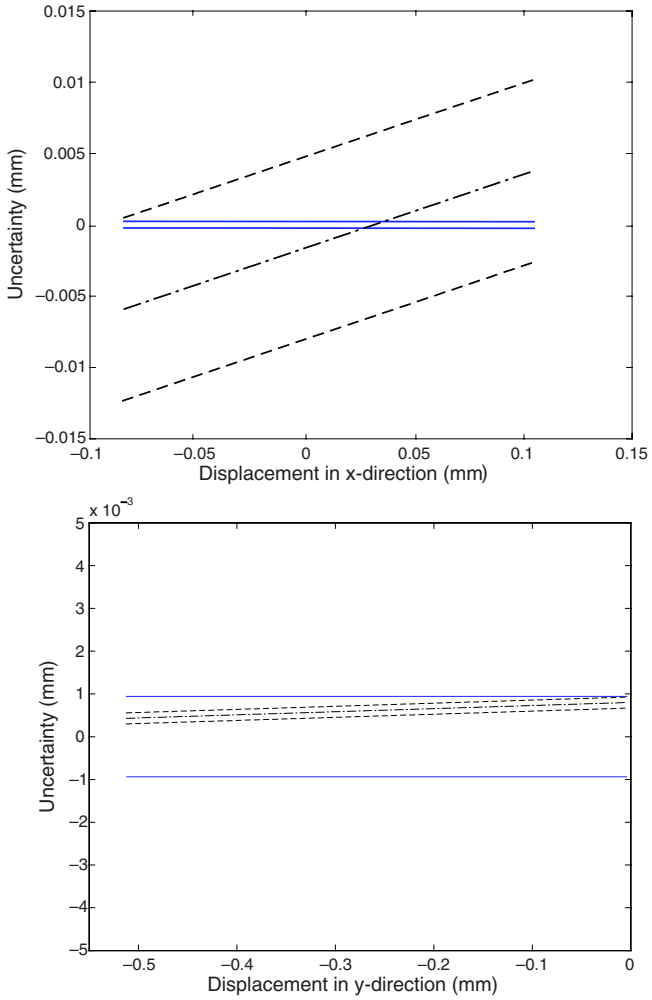

Figure 8. Comparison of expanded uncertainty in the theoretical predictions, $\pm 2\,u(mT)$ (solid lines) and field of deviations from the measurements, $\alpha + \beta m^T \pm 2u(d)$ (dashed lines) as function of the measurand, m_x^E (top) and m_y^E (bottom) for the in-plane bending case.

fringe projection and 2D digital image correlation system. In order to make comparisons between calibrations it is convenient to express the calibration uncertainty as a percentage of the maximum range of the measurand, $\widehat{m}$ to produce a relative uncertainty expressed as a percentage. The relative uncertainties obtained in this study are less than 3% for the in-plane static and mode 1 out-of-plane dynamic cases and about 6% for the mode 2 out-of-plane dynamic case which is comparable to those obtained by Felipe-Sesé *et al* for out-of-plane measurements. However, their in-plane measurements exhibited a much larger relative error of 16%, which was probably due to the very small in-plane deformation that occurs when the cantilever is subject to out-of-plane bending. These small deformations are likely approaching the noise level in the measurements and hence make calibration impractical.

For this reason, the cantilever reference material was subjected to in-plane bending in this study to generate larger in-plane displacements, as can be seen in table 3. The calibrations with the SPOTS reference material were focused on strain measurements rather than displacements and so again the use of relative uncertainties for comparison is useful. The range of relative uncertainty for in-plane measurement in this study is from 0.1% to 1.3%, which is better than the range obtained by Sebastian and Patterson [9], who obtained a range of 1.4% to 4.8% for 2D-DIC measurements with the SPOTS reference material, and rather better than the range of 2.2% to 6.2% obtained by Whelan *et al* [8] for ESPI measurements on the SPOTS reference material. Of course, this could imply that measurements from the ESPI system were inherently more uncertain than those obtained from the DIC systems. However, it seems reasonable to conclude that the reference material used in this study provides results that are at least as good as those produced with the SPOTS reference material, particular if in-plane, rather than out-of-plane, loading is employed when assessing in-plane measurement uncertainties.

For in-plane static bending the values obtained in this study for offset α, slope error β and residual $u(d)$, see equations (9)–(12), are given in tables 2 and 3, while they are displayed in the form $\alpha + \beta m^T \pm 2u(d)$ in figure 8. The y-displacement (load direction) has an offset of 0.8 μm, a slope error of less than 0.1% and a residual of less than 0.1 μm, leading to a relative uncertainty of 0.1% full scale (table 3). In contrast, the x-displacement has an appreciable offset of $-1.6\,\mu$m, a slope error of 5% adding $\pm 5\,\mu$m for a range of $\pm 100\,\mu$m and a residual of 3.2 μm. Although this can still be considered acceptable based on the comparison in figure 8 where the measurements uncertainties completely overlap with the uncertainty in the predictive values, it is recommended that a more robust calibration would be obtained using only the y-displacements and that the measurement system or reference material should be rotated by 90° to allow a calibration on the other axis of the system, as also proposed in the SPOTS protocol [6].

In the dynamic experiments, the results from the first two modes of vibration were presented. For the first mode, two different measurement ranges were shown. This was done in order to provide a relatively large displacement example (290 μm) and one which was of the same order of magnitude as the measurement from the second mode, i.e. 90 μm compared to 42 μm which was the largest amplitude that could be obtained with the loudspeaker and reference material used in these experiments. The offset was less than 0.5 μm, while the slope error was less than 1% for the first mode but 5% for the second. The residual across the three measurements was consistent and ranged from 2.2 to 2.9 μm. As the amplitude was different for each of the measurements, the relative uncertainty spanned a larger range, from 1.0% at the 290 μm range of the first mode to a maximum of 6.0% for the 42 μm range of the second mode. The plot of $\alpha + \beta m^T \pm 2u(d)$ in figure 9 shows that the deviations are comparable to the uncertainty of the predicted values and overlapping. The results presented here are comparable to the 2.4% relative uncertainty reported by Felipe-Sesé *et al* [11] for static out-of-plane bending of the cantilever.

Although the values for offset α and slope error β are significantly distinct from zero in all cases, as seen from a comparison to their uncertainties $u(\alpha)$ and $u(\beta)$, they do not show a correlation with the sign or level of displacement. In addition, they do not compromise the overlap with the

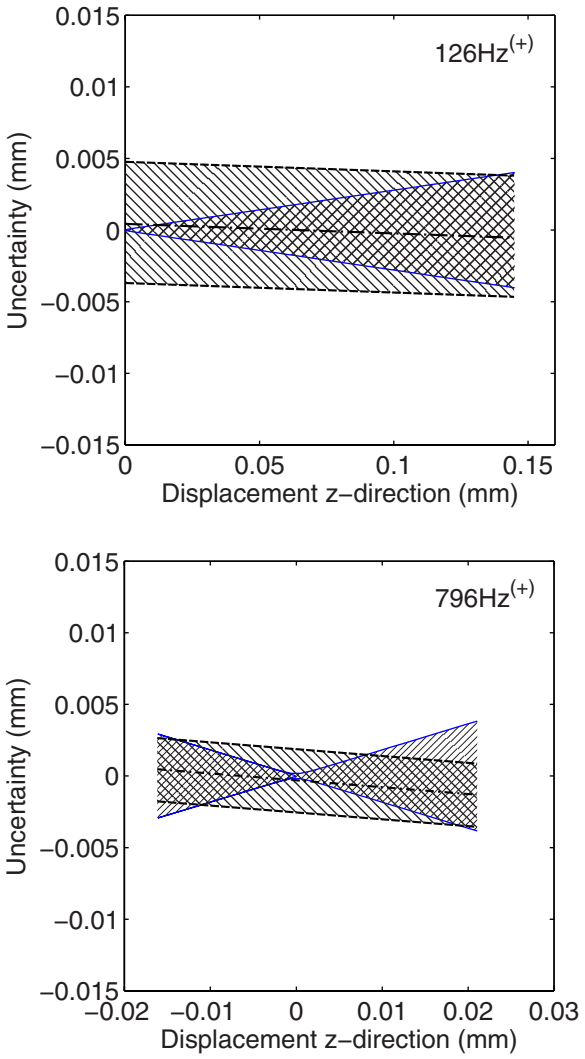

Figure 9. Comparison of expanded uncertainty in the theoretical predictions, $\pm 2\,u(m_z^T)$ (solid lines) and field of deviations from the measurements, $\alpha + \beta m_z^T \pm 2u(d)$ (dashed lines) as function of the measurand, m_z^E for the first (top) and second (bottom) mode corresponding to frequencies of 126 Hz and 796 Hz, respectively, for the out-of-plane case (only the positive z-direction data are shown).

uncertainty bands of the predicted values of the reference material, in figures 8 and 9, and therefore the need for a re-calibration is not indicated.

The underlying basis for the assessment of calibration uncertainty is the comparison with the displacements predicted from analytical theory. In this regard the reference material used in this study has a significant advantage compared to the SPOTS reference material, because no correction to the analytical theory is required to account for the effect of the boundary conditions. Although care needs to be taken not to collect data too close to the change in section at the root of the cantilever where the effect of the geometric discontinuity is not accounted for by the analytical expressions used to predict the displacements. In this work data was collected for an area of about 156 mm × 40 mm within the gauge area such that neither extremity at the root or the tip were included. The influence of the uncertainty in the input parameters on the predicted displacements has been accounted for by incorporating $u(m^T)$ into the evaluation of the calibration uncertainty. For the in-plane bending these parameters included the tip deflection as well as the dimensions and Poisson's ratio of the reference material, whereas for the dynamic measurements, $u(m^T)$ was influenced only by the uncertainty arising from the tip deflection measurement which in turn was a combination of the vibrometer measurement uncertainty, $u(\delta_z)$, and the relative positioning uncertainty, $u(\xi)$, i.e. it was independent of the dimensions of the reference material.

In this study, calibration uncertainties have been evaluated over a range of displacements and, in the case of dynamic loading, a range of frequencies. It has been concluded, based on the data shown in figures 8 and 9, that the experimental set-ups employed provide data of acceptable quality and that the calibration uncertainties can be regarded as the minimum uncertainties that could be expected in future measurements employing the identical set-up. If the set-up were changed, or different displacement or frequency ranges were considered then the calibration process would need to be repeated to establish the appropriate minimum measurement uncertainty.

6. Conclusions

The use of cantilever reference material to evaluate the minimum measurement uncertainty of an optical system for measuring static in-plane and dynamic out-of-plane displacement fields has been assessed by employing 3D digital image correlation as the exemplar measurement technique. It has been established that the cantilever reference material is easier to manufacture, requires no correction factors when predicting displacement fields, is more versatile and provided comparable results compared to the SPOTS reference material proposed previously.

Minimum measurement uncertainties for both a conventional and high-speed 3D digital image correlation system were found to be less than 3% for in-plane and less than 3 μm for the out-of-plane displacements. These uncertainties were evaluated using a protocol established previously for the SPOTS reference material [6] and embedded in a recent CEN Workshop Agreement [5] with modifications to allow for the application of in-plane bending loads.

It is concluded that the approach employed in this study provides a relatively straightforward route for practitioners to assess the minimum measurement uncertainty of camera-based optical systems for measuring displacement fields.

Acknowledgments

The dynamic experiments and analyses were part of an effort sponsored by the Air Force Office of Scientific Research, Air Force Material Command, USAF, under grant number FA8655-11-1-3083. The US Government is authorized to reproduce and distribute reprints for government purpose notwithstanding any copyright notation thereon. This work has received funding from the European Community's Seventh Framework Programme under Grant Agreement no. NMP3-SA-2012–319116. E A Patterson was the recipient of a Royal Society Wolfson Research Merit Award.

Appendix

Expressions for the partial derivatives in equations (16) and (17):

$$\left(\frac{\partial_y m_x}{\partial\delta}\right) = \frac{m_x}{\delta_y} = \frac{5y(-3(1+\nu)W^2 + 12Lx - 6x^2 + 2(2+\nu)y^2)}{L(20L^2 + (12+11\nu)W^2)} \tag{A.1}$$

$$\left(\frac{\partial m_x}{\partial L}\right) = \delta_y \frac{5y[(36+69\nu+33\nu^2)W^4 + (180(1+\nu)L^2 + (72+66\nu)x^2 - (48+68\nu+22\nu^2)y^2)W^2 + 120(3x^2 - 4Lx - (2+\nu)y^2)L^2]}{L^2(20L^2 + (12+11\nu)W^2)^2} \tag{A.2}$$

$$\left(\frac{\partial m_x}{\partial W}\right) = \delta_y \frac{20Wy[3(12+11\nu)x^2 - 30(1+\nu)L^2 - (72+66\nu)Lx - (24+34\nu+11\nu^2)y^2]}{L(20L^2 + (12+11\nu)W^2)^2} \tag{A.3}$$

$$\left(\frac{\partial m_x}{\partial \nu}\right) = \delta_y \frac{5y[-3W^4 + (66x^2 - 60L^2 - 132Lx - 20y^2)W^2 + 40L^2y^2]}{L(20L^2 + (12+11\nu)W^2)^2} \tag{A.4}$$

$$\left(\frac{\partial m_x}{\partial x}\right) = \delta_y \frac{60y(L-x)}{L(20L^2 + (12+11\nu)W^2)} \tag{A.5}$$

$$\left(\frac{\partial m_x}{\partial y}\right) = \delta_y \frac{15(4Lx - 2x^2 + 2(2+\nu)y^2 - (1+\nu)W^2)}{L(20L^2 + (12+11\nu)W^2)} \tag{A.6}$$

$$\left(\frac{\partial_y m_y}{\partial\delta}\right) = \frac{m_y}{\delta_y} = \frac{10(3L-x)x^2 + (12+11\nu)W^2x + 30(L-x)\nu y^2}{L(20L^2 + (12+11\nu)W^2)} \tag{A.7}$$

$$\left(\frac{\partial m_y}{\partial L}\right) = \delta_y \frac{[-((144+264\nu+121\nu^2)x)W^4 + 10(x^3 - 6L^2x + 3\nu xy^2)(12+11\nu)W^2 + 600(x^3 - 2Lx^2 + 3\nu xy^2 - 2\nu Ly^2)L^2]}{L^2(20L^2 + (12+11\nu)W^2)^2} \tag{A.8}$$

$$\left(\frac{\partial m_y}{\partial W}\right) = \delta_y \frac{20\,W(12+11\nu)(-3\nu Ly^2 + 3\nu xy^2 + 2L^2x - 3\,Lx^2 + x^3)}{L(20L^2 + (12+11\nu)W^2)^2}$$

$$\left(\frac{\partial m_y}{\partial \nu}\right) = \delta_y \frac{10[(11x^3 - 33Lx^2 + 22L^2x - 36xy^2 + 36Ly^2)W^2 + 60(Ly^2 - xy^2)L^2]}{L(20L^2 + (12+11\nu)W^2)^2} \tag{A.9}$$

$$\left(\frac{\partial m_y}{\partial x}\right) = \delta_y \frac{((12+11\nu)W^2 - 30(x^2 - 2Lx + \nu y^2))}{L(20L^2 + (12+11\nu)W^2)} \tag{A.10}$$

and

$$\left(\frac{\partial m_y}{\partial y}\right) = \delta_y \frac{60\nu y(L-x)}{L(20L^2 + (12+11\nu)W^2)}. \tag{A.11}$$

References

[1] Bayarri M J, Berger J, Paulo R, Sacks J, Cafeo J, Cavendish J, Lin C-H and Tu J 2007 A framework for validation of computer models *Technometrics* **49** 138–54

[2] AMSE V&V 10-2006 *Guide for the Verification and Validation of Computational Fluid Dynamics Simulations* (New York: ASME)

[3] Oberkampf W L and Barone M F 2006 Measures of agreement between computation and experiment: validation metrics *J. Comput. Phys.* **217** 5–36

[4] Sebastian C, Hack E and Patterson E A 2013 An approach to the validation of computational solid mechanics models for strain analysis *J. Strain Anal.* **48** 36–47

[5] Validation of computational solid mechanics models 2014 *Comité Européen de Normalisation (CEN), CEN Workshop Agreement* CWA 16799: 2014

[6] Patterson E A, Hack E, Brailly P, Burguete R L, Saleem Q, Siebert T, Tomlinson R A and Whelan M P 2007 Calibration and evaluation of optical systems for full-field strain measurement *Opt. Lasers Eng.* **45** 550–64

[7] ISO/IEC Guide 99 *International Vocabulary of Metrology—Basic and General Concepts and Associated Terms*

(VIM) Joint Committee for Guides in Metrology 200: 2008
[8] Whelan M P, Albrecht D, Hack E and Patterson E A 2008 Calibration of a speckle interferometry full-field strain measurement system *Strain* **44** 180–90
[9] Sebastian C M and Patterson E A 2015 Calibration of a digital image correlation system *Exp. Tech.* **39** 21–9
[10] Tan X, Kang Y L and Patterson E A 2012 Calibration of a 3D digital image correlation system for large deformation contact problems *J. Phys.: Conf. Ser.* **382** 012035
[11] Felipe-Sesé L, Siegmann P, Díaz F and Patterson E A 2014 Integrating fringe projection and digital image correlation for high-quality measurements of shape changes *Opt. Eng.* **53** 044106
[12] Pan B, Qian K, Xie H and Asundi A 2009 2D digital image correlation in in-plane displacement and strain measurement: a review *Meas. Sci. Technol.* **20** 062001
[13] Haddadi H and Belhabib S 2008 Use of rigid-body motion for the investigation and estimation of the measurement errors related to digital image correlation technique *Opt. Lasers Eng.* **46** 185–96
[14] Bornert M *et al* 2009 Assessment of digital image correlation measurement errors: methodology and results *Exp. Mech.* **49** 353–70
[15] Fazzini M, Mistou S, Dalverny O and Robert L 2010 Study of image characteristics on digital image correlation error assessment *Opt. Lasers Eng.* **48** 335–9
[16] Lava P, Cooreman S, Coppieters S, De Strycker M and Debruyne D 2009 Assessment of measuring errors in DIC using deformation fields generated by plastic FEA *Opt. Lasers Eng.* **47** 747–53
[17] Lava P, Cooreman S and Debruyne D 2010 Systematic errors in strain fields obtained via DIC using heterogeneous deformation generated by plastic FEA *Opt. Lasers Eng.* **48** 457–68
[18] Wang Y, Lava P, Coppieters S, De Strycker M, van Houtte P and Debruyne D 2012 Investigation of the uncertainty of DIC under heterogeneous strain states with numerical tests *Strain* **48** 453–62
[19] Becker T, Splitthof T, Siebert T and Kletting P 2006 Error estimations of 3D digital image correlation measurements *Technical Report* T-Q-400-Accuracy-3DCORR-003-EN, Dantec Dynamics GmbH, Ulm, Germany
[20] Sutton M A, Yan J H, Tiwari V, Schreier H W and Orteu J J 2008 The effect of out-of-plane motion on 2D and 3D digital image correlation measurements *Opt. Lasers Eng.* **46** 746–57
[21] Lava P, Coppieters S, Wang Y, van Houtte P and Debruyne D 2011 Error estimation in measuring strain fields with DIC on planar sheet metal specimens with a non-perpendicular camera alignment *Opt. Lasers Eng.* **49** 57–65
[22] Siebert T, Becker T, Splitthof K, Neumann I and Krupka R 2007 High-speed digital image correlation: error estimations and application *Opt. Eng.* **46** 051004
[23] Reu P 2013 A study of the influence of calibration uncertainty on the global uncertainty for digital image correlation using a Monte Carlo approach *Exp. Mech.* **53** 1661–80
[24] Zappa E, Mazzoleni P and Matinmanesh A 2014 Uncertainty assessment of digital image correlation method in dynamic applications *Opt. Lasers Eng.* **56** 140–51
[25] Reddy J N 1997 On locking-free shear deformable beam finite elements *Comput. Methods Appl. Mech. Eng.* **149** 113–32
[26] Astley R J 1992 *Finite Elements in Solids and Structures: an Introduction* (London: Chapman and Hall)
[27] Timoshenko S and Goodier J N 1951 *Theory of Elasticity* (New York: McGraw-Hill)
[28] Blevins R 1979 *Formulas for Natural Frequency and Mode Shape* (Princeton, NJ: Van Nostrand-Reinhold)
[29] Taylor B N and Kuyatt C E 1994 *Guidelines for Evaluating and Expressing the Uncertainty for NIST Measurement Results NIST Technical Note* 1297
[30] Sutton M A, Orteu J J and Schreier H 2009 *Image Correlation for Shape, Motion and Deformation Measurements: Basic Concepts, Theory and Applications* (Berlin: Springer)
[31] Tan X, Kang Y and Patterson E A 2014 An experimental study of the contact of a rounded rigid indenter with a soft material block *J. Strain Anal.* **49** 112–21
[32] ISO/IEC Guide 98 *Guide to Expression of Uncertainty in Measurement (GUM)* Joint Committee for Guides in Metrology 100:2008
[33] Ma D, Ong C W, Wong S F and He J 2005 New method for determining Young's modulus by non-ideally sharp indentation *J. Mater. Res.* **20** 1498–506